Electron Channeling Contrast Imaging: Rapid Characterization of Semiconductors

Julia I. Deitz[1]

Introduction

For semiconductor technologies, achievement of their ultimate potential depends greatly upon the ability to fully harness and exploit their advanced properties, which in turn depends on understanding these properties and their limiters. As such, the detailed characterization and analysis of advanced semiconductor materials and structures is paramount for the elucidation of these fundamental structure-property relationships. With respect to the investigation of micro- to nano-scale features, which greatly impact the larger scale (i.e. bulk- and device-level) properties of most materials systems, electron microscopy is well-known to provide the kind of important, detailed information that no other class of techniques can match. Characterization of this sort is provides vital feedback into ongoing and future materials and device design, synthesis, and test efforts. To this end, the research described herein utilizes an emerging electron microscopy technique, electron channeling contrast imaging (ECCI), for the rapid microstructural characterization epitaxial semiconductor materials as applied toward three novel applications: imaging dislocations (crystalline defects) at a lattice-mismatched interface, visualization of phase separation within an unstable alloy, and investigating embedded (subsurface) epitaxial quantum dots (QD).

Transmission electron microscopy (TEM) has historically been the go-to method used for the detailed microstructural characterization of nearly all materials systems, including the epitaxial semiconductor materials of interest here, as it has the necessary resolution and sensitivity to accurately study such systems. However, sample preparation for TEM work can be

[1] Co-authors: Dr. Santino D. Carnevale, Dr. Steven A. Ringel, Dr. David W. McComb, and Dr. Tyler J. Grassman.

time intensive, often becoming a low-throughput bottleneck within such materials research. Additionally, TEM specimen preparation can often damage the sample and features of interest, compromising their integrity and the resultant data collected. Furthermore, the specimen sizes obtained for TEM analysis are typically very small (approximately 100 μm^2), which can be inadequate to ensure statically relevant representation of the sample as a whole.

ECCI has begun to gain attention as an alternative to traditional TEM characterization for the imaging of extended defects in crystalline (and polycrystalline) materials. One of ECCI's major advantages is that it can be performed within nearly any field-emission scanning electron microscope (SEM) equipped with either a backscattered electron (BSE) or forescattered electron (FSE) detector; such setups are quite common, and the BSE geometry is used here. The BSE ECCI signal is composed of electrons that have been inelastically scattered away from the incident in-going electron beam, with successive scattering events leading to the eventual departure of the electron from the sample surface, enabling its detection. BSEs mostly come from near the surface of the sample (i.e. up to around 100 nm deep) because the probability of backscattering to the detector decreases with penetrating depth.

Like TEM, ECCI allows for imaging at specific diffraction conditions, determined through the use of low-magnification electron channeling patterns (ECP).[1] ECPs provide an orientation-space representation of incident electron beam diffraction, effectively yielding an angular map of the conditions where Bragg's law is met. Similar to two-beam imaging in TEM, ECCI can be performed at specific diffraction conditions by positioning the SEM's optic axis, via adjustment of the tilt and/or rotation of the crystal, at the inflection of the Kikuchi band/line of the target index; this places the crystal in position such that a well-defined Bragg condition is produced between the crystal and the incident electron beam. Once at a desired diffraction

condition, the user can simply zoom in (i.e. increase magnification), and any deviations from the bulk diffraction condition will provide imaging contrast. Essentially, this ability for ECCI to achieve diffraction conditions with the BSE detector is what makes it possible to detect subsurface features.

Keeping the imaging similarity with TEM in mind, ECCI's ultimate advantage then comes from the fact that this can all be done without the need for extensive sample preparation. Because the electrons do not transmit through the sample, as in TEM, thinning the specimen to electron transparency is completely unnecessary and bulk or as-grown samples can be used. This also helps to preserve the original nature of the sample under study (e.g. no thinning induced damage). The backscattered nature of the detected signal does necessitate a relatively smooth surface, but this is typically available with epitaxial samples; if not, the sample can be polished or gently ion-milled to reduce the roughness. Additionally, since ECCI is performed in an SEM, large area analysis is possible. With TEM, there is a limited scope of available information due to the small specimen size; the large analysis areas possible via ECCI help eliminate questions of statistical relevance that exist with TEM. In fact, ECCI can be performed over areas limited only by the geometry of the SEM, meaning that sample sizes ranging up to full wafers are applicable, allowing for the straightforward investigation of larger trends within samples.

To date, ECCI has predominantly been used to image dislocations that are either on or very near a sample's surface, such as surface-penetrating dislocations in metals[2] and semiconductor materials, such as GaN[3] and SiC.[4] This limitation is based upon the fact that, as previously mentioned, the ECCI signal is ultimately made up of inelastically backscattered electrons, resulting in a high degree of near-surface sensitivity. Moving beyond that, ECCI has recently been used to image crosshatch at buried heterointerfaces between lattice mismatched

materials in a small number of reports, including lattice-mismatched InGaAs/GaAs[5] and SiGe/Si.[6]

In this contribution, applications of ECCI are expanded through its use toward three novel applications. First, ECCI is used specifically for the characterization of defects within heteroepitaxial samples of GaP grown on Si(100) substrates,[7] in order to develop a better understanding of the dislocation dynamics in this materials system. To the authors' knowledge, this is the first extensive application of this technique for imaging and analysis of misfit dislocations and their dynamics at the interface of lattice-mismatched materials, as well as the first application to this particular material system. Also presented here are preliminary results regarding the further expansion of ECCI as applied to other epitaxial (opto)electronic materials systems, including the first demonstrations of the use of ECCI for the visualization of subsurface epitaxial III-V QDs (InAs/GaAs) and the detection and characterization of crystallographic defects and phase separation in a III-V alloy (InGaP).

Experimental Details:

Samples presented here were grown in-house. The GaP/Si samples in this work were grown by metal-organic chemical vapor deposition (MOCVD) in an Aixtron 3x2" close-coupled shower head system using 4" Si(100) wafers offcut 6° toward [011]. Details regarding the process used have been published previously.[8]

The InAs/GaAs QD samples were grown via molecular beam epitaxy (MBE) at 500°C. A single layer of QDs was produced via the deposition of ~1.6 ML InAs and subsequently capped with 30 nm of GaAs. No surface layer of QDs was grown. Previous identical growths that did

included terminal surface analysis layers yielded QDs with a range of about 3.5 – 4.2 nm in height and 30 – 35 nm base width (via atomic force microscopy, AFM).

The InGaP samples were grown by MOCVD at 650°C. The particular sample discussed here was an early calibration growth targeting a composition of $In_{0.44}Ga_{0.56}P$ (lattice-matched to a tensile-graded $GaAs_{0.90}P_{0.10}/GaAs_yP_{1-y}/GaAs$ virtual substrate). X-ray diffraction (XRD) reciprocal space mapping (RSM), such as that shown in Figure 2(a), revealed the presence of two distinct InGaP-related peaks that were tensile-strained with respect to the target $GaAs_{0.90}P_{0.10}$ lattice constant, indicating lattice-mismatch (i.e. missed composition) and suggesting phase separation. This is most likely the result of the lattice misfit strain and non-optimal growth conditions (i.e. temperature and rate) within a range known to yield phase instabilities.[9]

The as-grown samples were cleaved into conveniently-sized (~1 cm^2) pieces and loaded into an FEI Sirion field-emission SEM, fitted with a pole piece mounted annular BSE detector, for ECCI analysis. The ECCI work presented herein was performed using an accelerating voltage of 30 kV, a spot size of 5 (~2.4nA beam current), and a working distance of 5 mm. The only exception to this is that the GaP/Si analysis was performed with an accelerating voltage of 25 kV.

Results and Analysis:

1. Application of ECCI to GaP/Si Interface

Epitaxial GaP on Si has been of interest for nearly four decades as a route for integration of III-V materials with Si substrates for high efficiency photovoltaic applications. This makes the GaP/Si system of particular interest for characterization because further progress in the optimization of the epitaxial processes – necessary for the achievement of photovoltaic quality

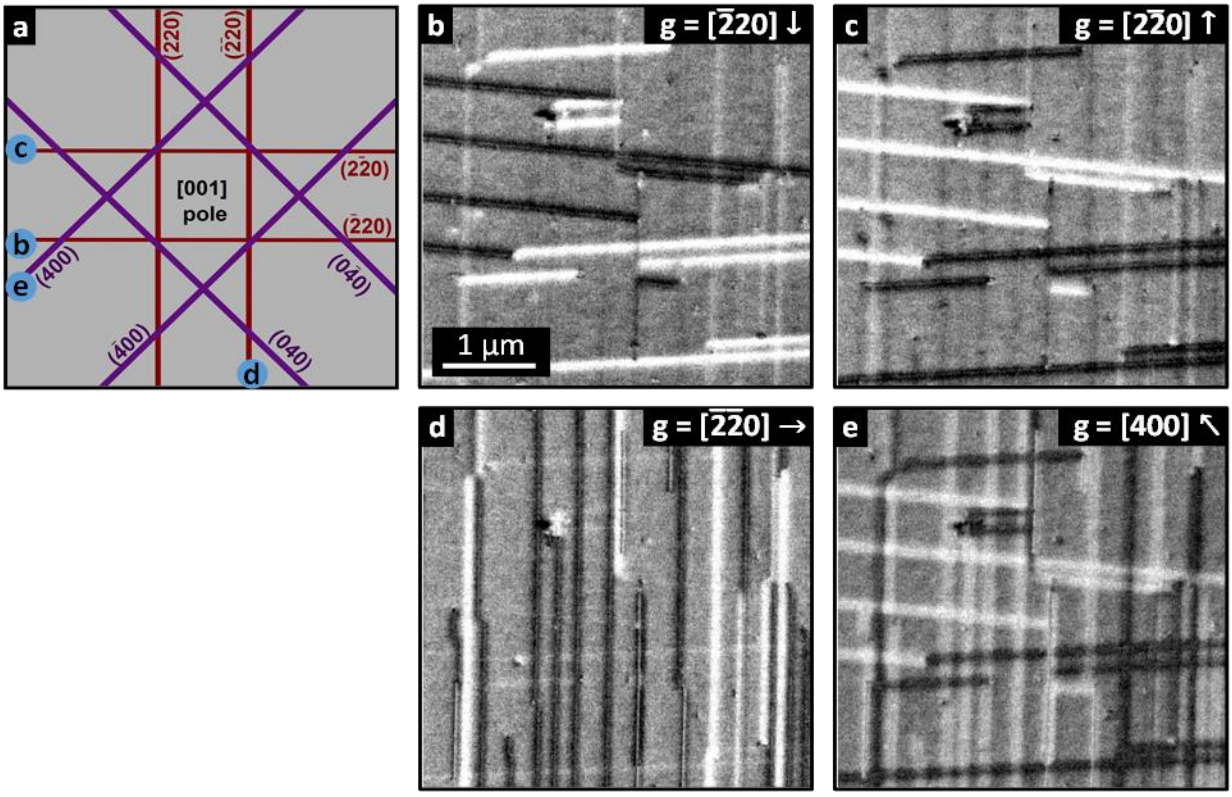

Figure 1: (a) Indexed illustration of a GaP ECP indicating the relative positions/diffraction conditions used for the ECCI images displayed in (b) – (e), which show misfit dislocations at the lattice-mismatched interface of a 50 nm thick GaP/Si sample. Respective **g** vectors are indicated for each image. Adapted from [7,10].

materials – requires a deeper understanding of the dislocation populations and dynamics, for which ECCI is ideally suited.

Example images of an interfacial misfit dislocation (MD) network in a 50 nm thick GaP-on-Si sample captured under different diffraction conditions are shown in Figure 1. The relative position of the optic axis on the ECP, as indicated by the diagram in Fig. 1(a), will determine the observed contrast of the defects, determined by the invisibility criteria. That is, just like in two-beam TEM, imaging contrast/visibility in ECCI is also determined by the standard invisibility criteria, or $\mathbf{g} \cdot (\mathbf{b} \times \mathbf{u}) = 0$ and $\mathbf{g} \cdot \mathbf{b} = 0$,[7,10] where **g** is the diffraction vector, **b** the Burgers vector, and **u** the defect/dislocation line direction. When the products are zero, the dislocation is not visible under the diffraction condition of interest, whereas when either product is non-zero, the dislocation should be visible, with contrast levels scaling to the magnitude of the products.

Physically, this phenomenon occurs because only crystal planes that are actually distorted by the dislocation – i.e. planes that are effectively non-orthogonal to those on which the dislocation resides – will result in electron scattering.

Fig. 1(b) is an image of the MD network under the **g** = $[\bar{2}20]$ condition. Following the invisibility criteria, MDs with Burgers vectors **b** = $[\bar{1}01]$ and = $[101]$ will show strong contrast because they are parallel to **g**, thus giving $|\mathbf{g} \cdot \mathbf{b}| >> 0$. Additionally, based on the second criteria, the horizontal **u** = $[\bar{1}\bar{1}0]$ line direction also gives large, non-zero values, reinforcing the strong contrast. On the other hand, those on the vertical **u** = $[\bar{1}10]$ direction yield $\mathbf{g} \cdot (\mathbf{b} \times \mathbf{u}) = 0$ for the same diffraction condition, but also $\mathbf{g} \cdot \mathbf{b} \neq 0$, and should thus provide only very weak contrast, as can be seen in Fig. 4(b). The opposite contrast levels (i.e. dark and bright) displayed by the MDs are also related to the specific value and polarity (i.e. positive vs. negative) of $\mathbf{g} \cdot \mathbf{b}$, thereby enabling a clear distinction between Burgers vectors of opposite sign. Figure 1(c) shows the same MD network with the diffraction condition **g** = $[2\bar{2}0]$. The same dislocations still possess high contrast, but of the opposite polarity due to the change in sign of the diffraction condition. This means that this contrast reversal can be used in combination with the known **g** vector to determine the sign of the Burgers vector, **b**, of a given defect; the same misfits that are perpendicular to **g** = $[\bar{2}20]$ are also perpendicular to **g** = $[2\bar{2}0]$. Indeed, the images were taken using the same Kikuchi band, but on opposite edges. In Figure 1(d), misfit dislocations that are orthogonal to those highlighted in Figs. 1(b)-(c) now exhibit strong contrast due to the use of a diffraction vector, **g** = $[220]$, which is orthogonal to those used in 1(b)-(c). In the final image, Fig. 1(e), both sets of MDs are visible when using a diffraction vector, **g** = $[400]$, which is not parallel (i.e. has some perpendicular character) to either set.

Clearly, these results indicate the importance of the diffraction condition on the available information in an image. Furthermore, this application of ECCI to investigate defects at an interface demonstrates its usefulness for epitaxial semiconductor research where it can save substantial amounts of time and effort, helping to accelerate not only basic research efforts, but targeted development projects, as well.

2. Application of ECCI to Complex III-V Alloys: Phase Separation

The InGaP ternary alloy system is of major importance to many optoelectronics applications, like LEDs and lasers, and nearly all III-V based photovoltaics (PV) technologies. This is because of the wide lattice constant range that it spans, while also possessing the largest available (non-Al containing) direct bandgaps over much of it. Nonetheless, the $In_xGa_{1-x}P$ alloy system is also fraught with complex issues, such as atomic ordering and significant phase instabilities (i.e. a miscibility gap over much of its compositional range). As such, $In_xGa_{1-x}P$ is also a prime candidate for rapid microstructural characterization methods.

Figures 2(b) and 2(c) present preliminary ECCI data taken from a metamorphic $In_xGa_{1-x}P$ epilayer calibration growth. Here a diffraction condition of **g** = [220] was used. The low

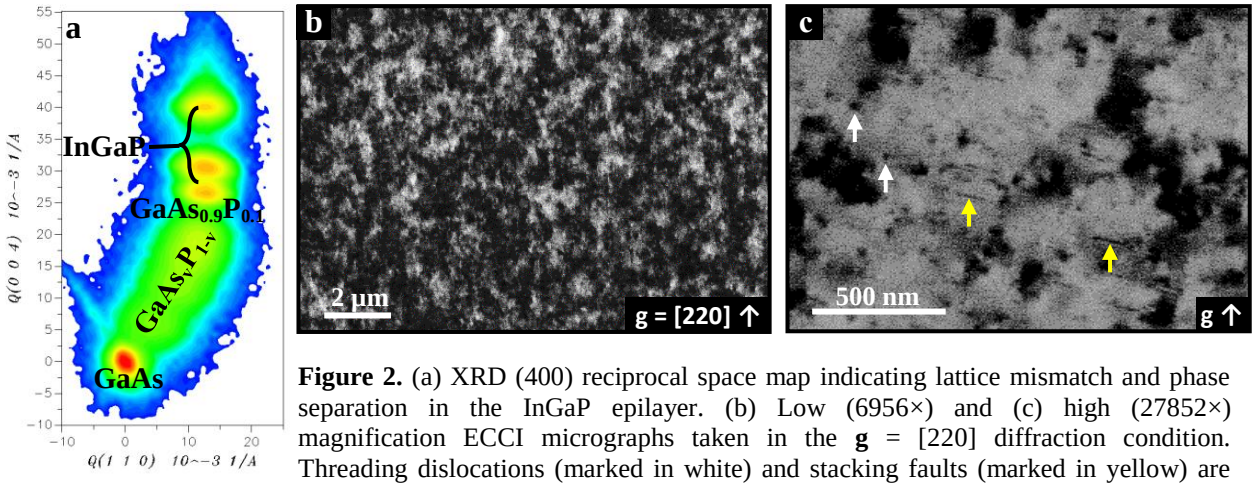

Figure 2. (a) XRD (400) reciprocal space map indicating lattice mismatch and phase separation in the InGaP epilayer. (b) Low (6956×) and (c) high (27852×) magnification ECCI micrographs taken in the **g** = [220] diffraction condition. Threading dislocations (marked in white) and stacking faults (marked in yellow) are identified in (c).

magnification image in Fig. 2(b) shows a strong mottled appearance – as opposed to the uniform background contrast seen in the GaP/Si based samples – with no apparent correlation to any surface structure. Given the indication of phase separation provided by the XRD (Fig. 2(a)), and the high sensitivity of ECCI to strain, the most likely source of this contrast is phase separation, where the two slightly lattice-mismatched phases possess different levels of strain, and thus slightly different angles needed to satisfy the [220] channeling Bragg condition. Indeed, two-beam TEM also yields a similar contrast appearance in the presence of phase separation, depending upon the degree and extent of the separation.[11] Work is in progress to verify the identification of phase separation via ECCI in this sample and others, including investigation of different imaging/diffraction conditions and complementary TEM.

Of additional note here is that in the high magnification micrograph in Fig. 2(c) a large number of crystal defects – e.g. threading dislocations and stacking faults – are visible. These defects are likely the result of both lattice mismatch and the resultant phase separation, which tends to amplify such issues. While this calibration growth has clearly resulted is a poor quality epilayer, the ability to visualize these defects despite the apparent phase separation, in addition to the general alloy scattering that also contributes to the degradation of the channeling quality, provides demonstration that ECCI is still a useful characterization technique even in crystalline materials that are highly non-uniform. This includes not only other III-V alloys with phase instabilities (e.g. InGaAs, InAlAs, InPSb, GaAsSb, etc.), but also potentially even more complex materials, such as thin-film chalcogenides. Indeed, ECCI has been previously used for characterization of even polycrystalline metals,[12] but similar applications to semiconductor materials have yet to be demonstrated.

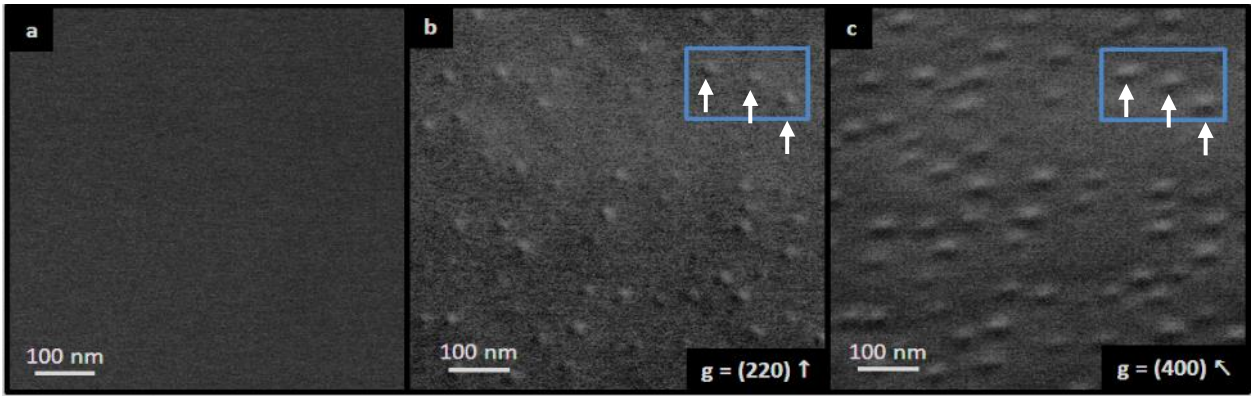

Figure 3. Single-layer InAs QDs in GaAs host as imaged via (a) standard surface-normal BSE, (b) **g** = [220] ECCI, and (c) **g** = [400] ECCI. The same region is picture in (b) and (c), and the blue rectangle surrounding three QDs, marked with arrows, provides frame of reference.

3. Application of ECCI to Epitaxial Quantum Dots

Epitaxial quantum dots (QDs) within the III-V compound semiconductor materials system typically form via the Stranski-Krastanov mechanism, a form of strain relaxation within lattice-mismatched thin films without the generation of dislocations. Upon encapsulation, the QDs exert a high degree of strain on the surrounding material, producing strong strain fields that should strongly scatter the channeling electrons (easily observable with traditional zone-axis or two-beam TEM). It is thus anticipated that ECCI should enable the imaging of embedded QDs in plan-view geometry.

To this end, Figure 3 presents ECCI micrographs of a single layer of InAs QDs embedded within a GaAs host at multiple imaging conditions: (a) standard surface-normal, surface-sensitive non-diffractive BSE geometry, (b) **g** = [220], and (c) **g** = [400]. Clearly visible in Figs. 3(b) and 3(c) are what appear to be small, round features consistent with the appearance of QDs, while the standard BSE image in Fig. 3(a) shows no significant surface features (confirmed by AFM). As previously discussed, when imaging typical crystalline defects, such as dislocations or stacking faults, the invisibility criteria determine what is seen at different

diffraction conditions. QDs should also demonstrate imaging contrast dependent upon this same criteria, but their quasi-isotropic, three-dimensional strain fields should be visible under a wide range of diffraction conditions, with some yielding higher contrast (i.e. related to strain magnitude) than others, consistent with what is seen in Figs. 3(b) and 3(c). Interestingly, the QDs appear larger in the **g** = [400] condition than in the **g** = [220] condition, which is consistent with stronger/larger QD-induced vertical strain fields versus lateral, as would be expected for the tetragonally distorted QDs.

With the combination of ECCI's capabilities for imaging crystallographic defects and this demonstration of QD imaging, ECCI could be a powerful tool in QD research, enabling rapid characterization of such aspects as embedded QD density, size/shape, and uniformity, as well as investigation of potential QD-induced defect formation.

Conclusions

Here, a brief introduction to ECCI is provided, along with examples of recent work toward the expansion and adaptation of this technique to a number of important applications in III-V epitaxial structures. This work demonstrates the use of ECCI for nondestructive characterization of misfit dislocations at the lattice-mismatched interface of heteroepitaxial GaP-on-Si samples, phase separation in complex alloys, and subsurface epitaxial QDs. These uses were specifically aimed at the characterization of materials and structures with application to photovoltaics and optoelectronics, but ECCI can be used for defect and feature analysis in many other types of crystalline materials and structures. In all cases the results are comparable to those achieved via TEM analysis, but with the advantage of little to no specimen preparation and the use of SEM instrumentation.

Acknowledgements

The author would like to acknowledge her collaborators – Drs. Santino Carnevale, Marc De Graef, and Steven Ringel – and her advisors – Drs. David McComb and Tyler Grassman – for their contributions to this work. This work was supported by the Department of Energy under the FPACE program (DE-EE0005398) and OSU's Institute for Materials Research.

References:

[1] D. Joy, D. Newbury, and D. Davidson, *J. Appl. Phys*. ***53***, R81, (1982).
[2] M. A. Crimp, *Microsc. Res. Tech.* ***69***, 374 (2006).
[3] Y. Picard, R. Kamaladasa, M. De Graef, N. Nuhfer, W. Mershon, T. Owens, L. Sedlacek, and F. Lopour, *Microsc. Today* ***20***, 12-16, (2012).
[4] Y. Picard, J. Caldwell, M. E. Twigg, C. R. Eddy, Jr., M. A. Mastro, R. L. Henry, and R. T. Holm, *Appl. Phys. Lett*. 91, 094106, (2007).
[5] A. Wilkinson, *Philos. Mag. Lett*. ***73***, 337-344, (1996).
[6] A. Wilkinson, G. Anstis, J. Czernuszka, N. Long, and P. Hirsch, *Philos. Mag. A*. ***68***, 59 (1993).
[7] S. Carnevale, J. Deitz, J. Carlin, Y. Picard, M. De Graef, S. Ringel, and T. Grassman, *Appl. Phys. Lett.* ***104***, 232111, (2014).
[8] T. Grassman, J. Carlin, B. Galiana, L.-M. Yang, F. Yang, M. Mills and S. Ringel, *Appl. Phys. Lett.* ***102****(14),* 142102 (2013).
[9] A. Kim and E. Fitzgerald, *Proc. SPIE* ***3621***, pp. 179-187, 1999.
[10] J. Deitz, S. Carnevale, S. Ringel, D. McComb, T. Grassman, *Journ. of Vis. Exp.*, 52745R2, (2015).
[11] N. Quitoriano, and E. Fitzgerald, *J. Appl. Phys.* ***102****(3)*, pp. 033511-033517, (2007).
[12] S. Zaefferer and N. Elhami, *Acta Mater.* ***75***, 20–50, (2014).